AN INVESTIGATION ON VERTICAL TAILPLANE DESIGN

Fabrizio Nicolosi
Dep. of Aerospace Engineering
University of Naples Federico II
Via Claudio, 21
80125 Napoli - Italy
fabrnico@unina.it

Pierluigi Della Vecchia
Dep. of Aerospace Engineering
University of Naples Federico II
Via Claudio, 21
80125 Napoli - Italy
pierluigi.dellavecchia@unina.it

Danilo Ciliberti
Dep. of Aerospace Engineering
University of Naples Federico II
Via Claudio, 21
80125 Napoli - Italy
dancili@gmail.com

Abstract. The paper presents a deep investigation on the methodologies to design a vertical tailplane. Nowadays the most used methodologies in preliminary design to estimate the contribution of vertical tailplane on aircraft directional stability and control are: the classical method proposed by USAF DATCOM (also presented in several aeronautics textbooks) and the method presented in ESDU reports. Both methodologies derive from NACA world war II reports of the first half of the '900, based on obsolete geometries, and give quite different results for certain configurations, e. g. in the case of horizontal stabilizer mounted in fuselage. As shown in literature, the main effects on the side force coefficient of the vertical tail are due to the interactions among the aircraft components: the fuselage acts like a cylinder increasing the local sideslip angle, the wing position and aspect ratio have an influence on the airflow near the tail zone and the horizontal tail, depending on position and size, can act as an endplate increasing the side force. In order to better highlight these effects, a different approach using the RANS equations has been adopted. Several CFD calculations have been performed on some test cases (used as experimental database) described in NACA reports and used in the past to obtain the semi-empirical methodology reported in USAF DATCOM, to verify the compliance of CFD results with available experimental data. The CFD calculations (performed through the use of a parallel supercomputing platform) have shown a good agreement between numerical and experimental data. Subsequently the abovementioned effects have been deeply investigated on a new set of propeller transport aircraft configurations. The different configurations that have been prepared differs for wing aspect ratio, wing-fuselage relative position (high-wing/low-wing), vertical tailplane aspect ratio (vertical tail span versus fuselage radius) and horizontal tailplane position respect to the vertical tailplane (in particular investigation the effect of fin-mounted T configuration, typical of regional turboprop transport aircraft). For all configurations the computational mesh has been carefully analyzed and prepared. All the CFD analyses will be useful to obtain new curves to predict the above-mentioned effects and to have a more accurate estimation of vertical tailplane contribution to aircraft directional stability and control.

Keywords. Vertical tailplane aerodynamics, directional stability, aircraft preliminary design

1 Introduction

Tailplane design needs an accurate determination of stability derivatives. The more accurate the latter the better the former. Nowadays the most known semi-empirical methods that estimate these derivatives are the USAF DATCOM[1] methodology, also presented by Roskam[2], and the ESDU[3] method. These are mainly based on NACA reports from the ‘30s to the ‘50s, contemplating obsolete geometries as elliptical bodies, swept wings and short fuselages (Figure 1), in contrast with the shape of the actual airliners; moreover they present non negligible discrepancies for certain configurations such as the horizontal tailplane mounted in fuselage. Both of them start from the definition of the isolated vertical tailplane lift curve slope $C_{L\alpha v}$ (the isolated vertical tail lift slope is usually evaluated according to the Helmuld-Diederich formula [2][4]) and modify it by means of corrective factors to obtain the final sideforce due to sideslip derivative $C_{Y\beta v}$. These semi-empirical factors provide for the effects of the fuselage, wing and horizontal tailplane on the vertical tailplane. Stability derivative $C_{N\beta v}$ and rolling moment derivative $C_{\mathcal{L}\beta v}$ are function of $C_{Y\beta v}$ tail position and angle of attack.

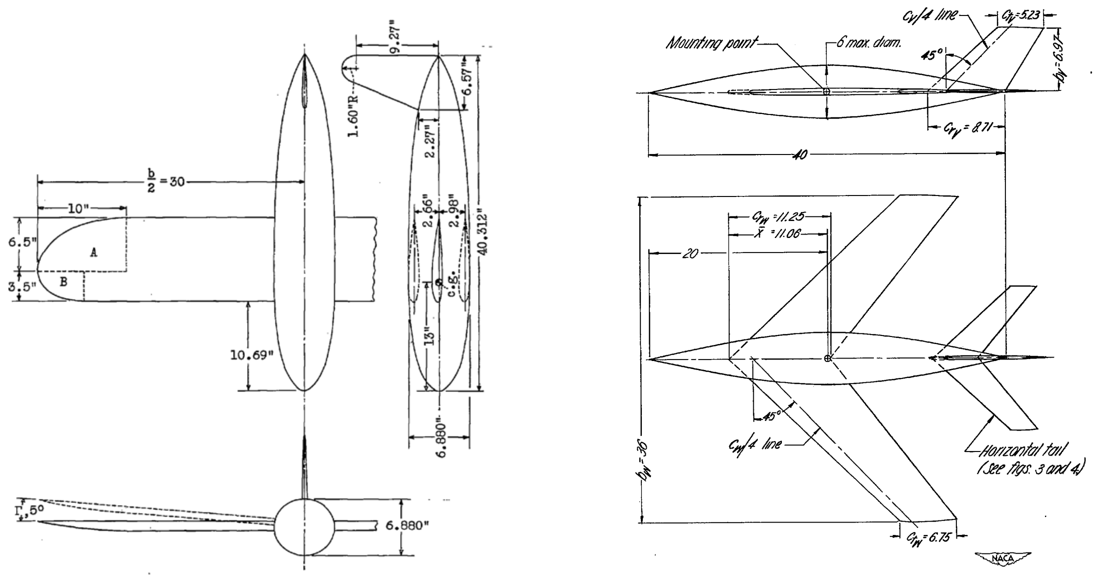

Figure 1: Some of the geometries used in NACA reports[8],[9].

In Section 2.1 a historical perspective of the NACA experimental investigation on the effects on the vertical tail is shown, highlighting the geometries and the combinations analyzed. Section 2.2 proposes an application of the above-mentioned semi-empirical approaches, with particular emphasis on the discrepancies between them.

Modern approaches make use of CFD, from panel methods to RANS. At DIAS (Department of Aerospace Engineering of the University of Naples Federico II), several analysis have been performed on the vertical tail using panel code methods[5]. Moreover panel method analysis shown a low capability to predict the effects of the wing wake on the vertical tail, especially in aircraft configurations with the body mounted horizontal tail.

The RANS approach is currently being investigated at DIAS, with the commercial CFD software Star-CCM+. More details will follow in Section 2.3.

Section 3 presents several test cases used to compare numerical calculations with NACA wind tunnel data both longitudinal and lateral directional.

Finally in Section 4 a deep investigation on several propeller aircraft configurations has been performed to evaluate the overall effects on the vertical tailplane.

2 A historical perspective

2.1 NACA experimental investigation

From the ’30s to the ’50s, in the USA, the National Advisory Committee for Aeronautics (NACA) provided some results on the directional stability on isolated vertical tailplanes, partial and complete aircraft configurations through many hours of wind tunnel tests, results that were summed up in a method of analysis completely reported and described in the USAF DATCOM[1]. The investigations strived to separate the effects of fuselage, wing and horizontal tail from the isolated vertical tail. Lots of geometries were tested, from the early years to the ’50s, i. e. rectangular, elliptical and swept wings, symmetrical and unsymmetrical airfoils, slender bodies with rounded or sharp edges, tails of different aspect ratio and size [6] to [10].

However the accuracy of these results were limited by the technology of the past years and, perhaps most important, they dealt with geometries quite different from the actual transport airplanes. As a matter of fact most of the work of the NACA was pushed by war and if the aim of the early tests was to gain a certain knowledge on the physics of the problem of directional stability and control[7] and on the mutual interference among aircraft components[6], later tests aimed to improve stability and maneuverability of high speed combat aircrafts[9]. A first effect studied (1939) by Bamber and House [8] was the aerodynamic interference of the wing-fuselage relative position on the vertical tail aerodynamic coefficients(see Figure 1). The general trend revealed an increase in sideforce due to sideslip coefficient $C_{Y\beta v}$ and yawing moment derivative $C_{N\beta v}$ when moving the wing from high to low position in fuselage, excepts for the fin-off combination where there was a minimum for the mid wing position (without the fin the model considered has double symmetry). This trend held when considering wing dihedral, flaps and angle of attack, though different values were achieved for each combination. The rolling moment derivative $C_{\mathcal{L}\beta v}$ decreased and changed sign as the wing was moved downward. The effect of the angle of attack on $C_{N\beta v}$ was very small and so for that geometry can be. The work of Bamber and House[8] does not consider the horizontal tail, so the interference effect on lateral stability was due to that particular wing-fuselage-fin combination. An interesting approach to evaluate the fuselage effect on the vertical tail was taken by Queijo and Wolhart[9]: an effective aspect ratio A_{ev} was defined and it was plotted against the ratio of vertical tail span b_v to the fuselage diameter d_f at the longitudinal location of the vertical tail aerodynamic center (shortly: tail span per body depth) and parameterized for various tail-fuselage combinations. The tail effectiveness increased as the ratio b_v/d_f decreased, that is as the tail became small compared to the fuselage. Theory (based on the assumption that the body acts as an endless plate at the base of the vertical tail) suggested a non linear increase of the effective aspect ratio with the ratio mentioned above. The scatter in experimental data became bigger with low b_v/d_f ratios and two different trend lines were drawn for two aspect ratios.

Before 1950 tests on straight wings and horizontal tails were made, but it was found by Brewer and Lichtenstein[10] that results could not be extended to swept planforms. The model used for the investigations[9][10](see also Figure 1) was designed to permit tests of the wing alone, fuselage alone, or the fuselage in combination with any of several tail configurations, with or without the wing. Details will follow in Section 2.3. In the work done by Queijo and Wolhart[9] the horizontal tail was not mounted. The effect of size and position of horizontal tail was studied by Brewer and Lichtenstein[10] (as shown in Figure 18). Here the fin-fuselage combination was ‘frozen’ and the effective lift curve slope of the isolated vertical tail was calculated. Here, the experimental lift-curve slope is about 13% higher than that predicted by theory. Indeed, according to the lifting surface theory, the gradient of the lift coefficient versus angle of attack curve is linear with aspect ratio for planforms with low aspect ratio (up to about 1.5).

All the previous experimental works performed at NACA were implemented in vertical tail design methodologies, the USAF DATCOM[1] and the ESDU[3].

2.2 Comparing semi-empirical methods

As it has been said before, the NACA experimental data were used to build up a methodology to estimate the sideforce coefficient of a generic vertical tail.

According to USAF DATCOM[1], resumed by Roskam[2], the sideslip derivative $C_{Y\beta v}$ is made up of three components: body cross-flow, horizontal surface, wing-body wake and sidewash effect (the latter two lumped into a single effectiveness parameter). The first two define an *effective* vertical tail aspect ratio to be substituted in the $C_{L\alpha v}$ formula (usually Helmuld-Diederich formula[2][4]) instead of the geometric aspect ratio then the lift gradient is corrected again by the sidewash effect and other semi-empirical factors.

The procedure proposed by ESDU[3] is quite simple: the sideslip derivative $C_{Y\beta v}$ is obtained by multiplying the vertical tail lift curve slope $C_{L\alpha v}$ by three semi-empirical factors that account for the effect of the fuselage, wing and horizontal tailplane. However, there's no wing wake effect, the sidewash is considered constant; moreover the geometric aspect ratio is differently defined.

In this section a comparison of the semi-empirical methods described above has been performed. Given the ATR-42 aircraft geometry, the vertical tail contribution to the sideforse has been estimated, as shown in Figure 2 black markers. As it can be seen the two methodologies for this aircraft give a quite similar results, with a difference of lower than 5%. To put in evidence the discrepancies between the two methods in Figure 2 the effect of changing the ratio between vertical tail span and fuselage thickness (on the left) and the horizontal tailplane position on the vertical tailplane (on right) has been shown. It is apparent that semi-empirical methods become less reliable for those configurations with very different results. More relevant differences can be observed on the zone of lower values of the $b_v/2r$ parameter(which is the ratio of vertical tail span b_v to the fuselage diameter d_f =2r at the longitudinal location of the vertical tail aerodynamic center) and on the extreme zone of the z_h/b_v parameter(which represents the horizontal tail position). a body mounted horizontal tail should give a difference between the two methodologies of the 24%, which should conduce to a completely different vertical tail design.

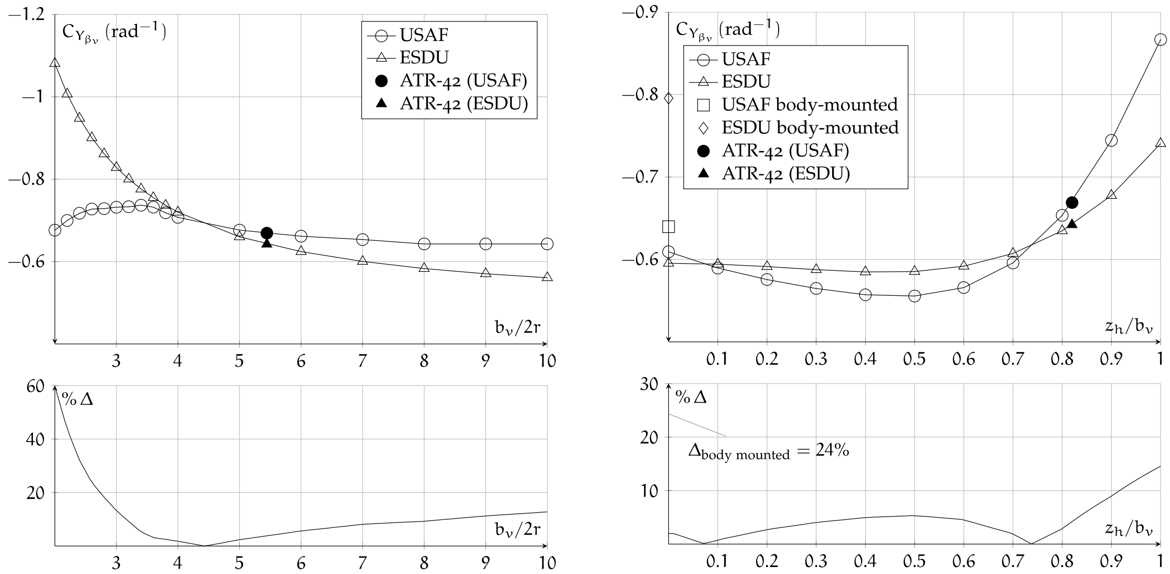

Figure 2: Sideforce derivative of the ATR-42 aircraft estimated through USAF and ESDU methodologies; effect of change the vertical tail span to fuselage thickness (left) and the horizontal tail position on vertical tail (right).

2.3 The CFD approach

The new approach adopted at the DIAS consists in the use of the commercial CFD software StarCCM+ to better investigate the whole effects on the vertical tail plane on a typical propeller aircraft. This software permits to work in an integrated environment, where it is possible to import (or generate, if the model is very simple) the CAD geometry, automatically generate a mesh, easily setup the physics, run the analysis and visualize the results as plots and scenes. One of its interesting features is the polyhedral cells mesh type: every cell is a polyhedral with an average of 14 faces. This permits a less number of cells in a numerical domain, thus saving memory used per CPU.

StarCCM+ was often used on the University's grid computing infrastructure (SCoPE) to simulate lots of configurations in a short amount of time. 128 licenses (one per CPU) were available for this investigation. Figure 3 on the left shows that doubling the CPUs number the time to convergence halves, while on the right shows some pictures of the fiber optic cables of SCoPE facility.

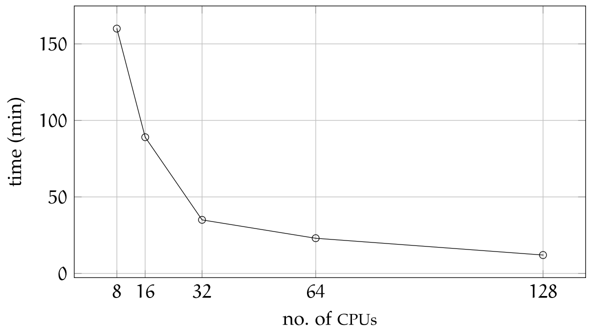

(a) *Linear plot*.

(a) *Three rack servers of the data center*.

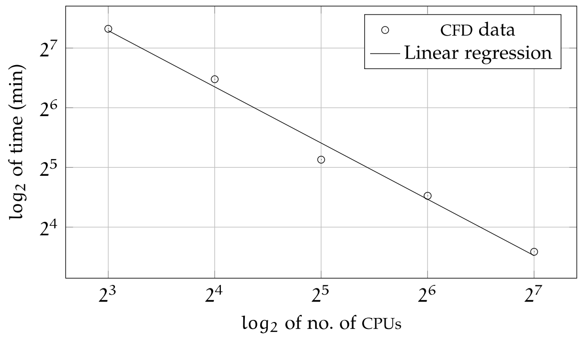

(b) *Logarithmic plot*.

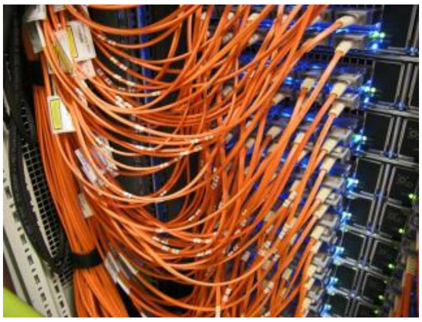

(c) *Fiber optic connections*.

Figure 3: Time vs. CPUs number (left) and the SCoPE grid infrastructure (right).

3 NACA test cases

In order to check the compliance of the CFD results with available test data, three test cases have been performed. These are a longitudinal test case and two directional test cases.

3.1 NACA report 540

In the work of Eastmen and Kenneth[11] 209 wing-fuselage combinations were tested in the NACA variable-density wind tunnel, to provide information about the effects of aerodynamic interference between wings and fuselage at a large value of the Reynolds number (3100000). The wing section is a NACA 0012 airfoil. Three of these combinations (respectively mid, high and low wing, marked no. 7, 22 and 67 in ref.[11]) plus a wing-alone configuration were chosen for the test case. In short, for each combination, a round fuselage with a rectangular wing has been analyzed at various angles of incidence, in symmetric flow. No discussion is made on the results since the primary interest of this section is the check of the previously stated compliance.

Results in terms of the aerodynamic lift, effective profile drag and moment coefficient C_L, C_{De} and C_M are shown, for the mid-wing combination, in Figure 4. Effective profile drag coefficient is defined as the difference between the total drag coefficient C_D and the minimum induced drag coefficient C_{Di}, as shown in Eq. 1;

$$C_{De} = C_D - \frac{C_L^{\ 2}}{\pi A} \qquad \text{Eq.1}$$

and this to account only for induced drag due to the interference of the wing-body combination. From the charts (only the mid-wing combination is shown) it is apparent the validity of the mesh and of the physics model involved (Spalart-Allmaras turbulence model), as the configurations at small angle of attack are well simulated by the CFD.

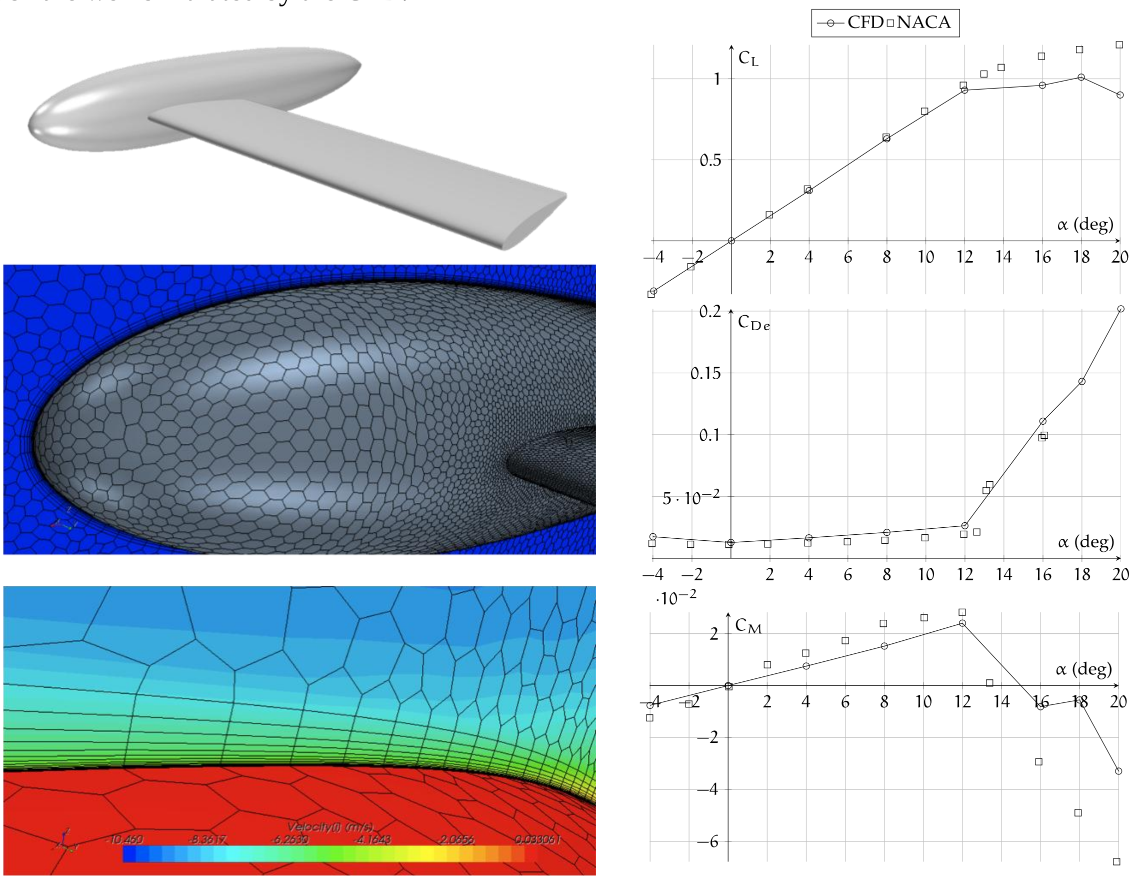

Figure 4: Results for the NACA report 540 (mid-wing combination) [11].

3.2 NACA report 730

In the report of Bamber and House[8], a NACA 23012 rectangular wing with rounded tips was tested with a round fuselage at several angles of sideslip, in a high, mid and low wing combination. Moreover each combination was tested with and without fin. The fin was made to the NACA 0009 section with an area of 45 sq. in. No dihedral angle and no flap device were considered. Reynolds number is 609000 based on wing chord. Results are evaluated in terms of the rolling moment, yawing moment and sideforce due to sideslip coefficients (for the whole configuration) $C_{\mathcal{L}\beta}$, $C_{N\beta}$ and $C_{Y\beta}$. All derivatives are per deg and evaluated assuming linearity with β between 0° and 5°. The chart shown in Figure 5 is for the wing-body fin configuration.

3.3 NACA report 1049

The aim of the work of Queijo and Wolhart [8] was to investigate the effects of vertical tail size and span and of fuselage shape and length on the static lateral stability characteristics of a model with 45°

swept back (quarter chord line) wing and vertical tail, NACA 65A008 airfoil. In this report is highlighted an interesting relation between the effective aspect ratio of the vertical tail and the fuselage thickness where the tail is located and this was resumed by the USAF DATCOM method. For the purpose of the test case, only a combination with a round fuselage was simulated. Results are shown in Figure 6 in terms of force and moment coefficients.

In conclusion, the results obtained with the CFD are close enough to the experimental results, so it appeared reasonable to use Star-CCM+ for the investigation on vertical tailplane design discussed in the next section.

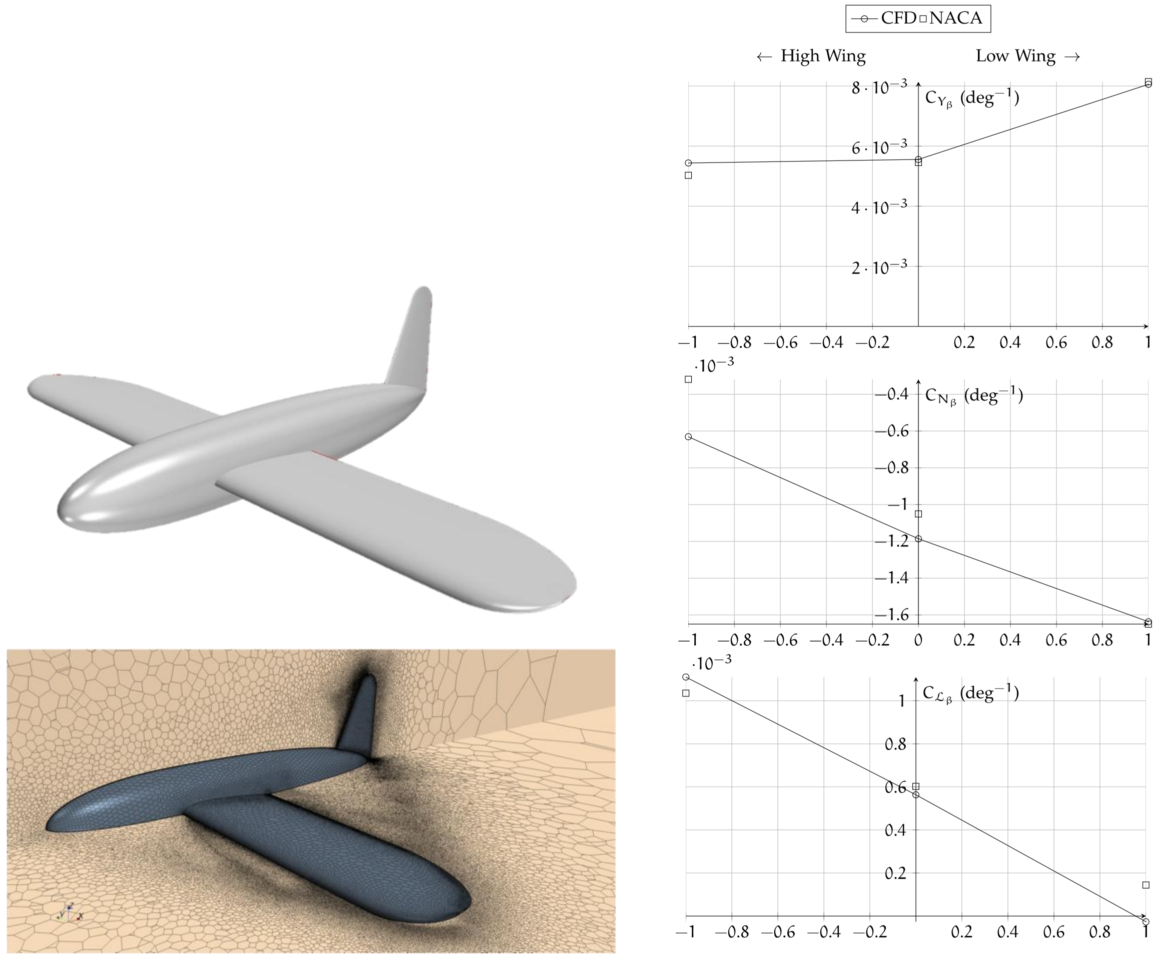

Figure 5: Results for the NACA report 730 (wing-body-fin combination)[8].

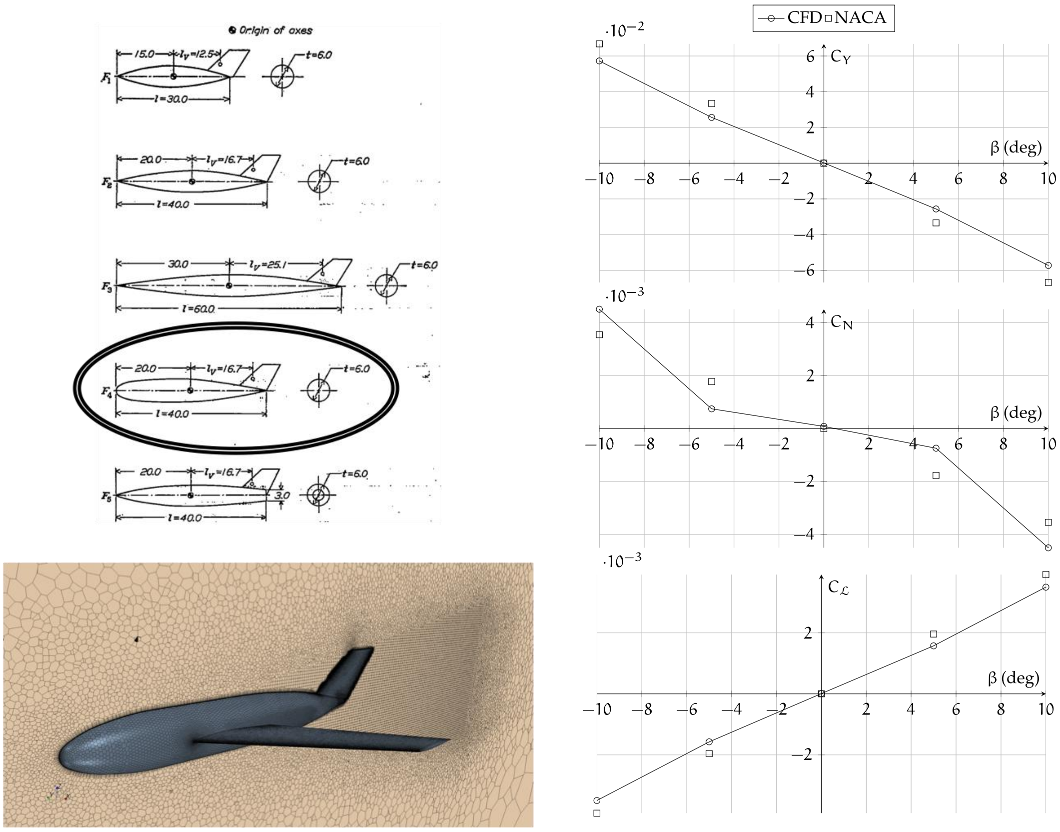

Figure 6: Results for the NACA report 1049 (wing-body-fin combination) [9].

4 A new investigation

An investigation on the interferences effects (on VT side-force derivative) illustrated in previous paragraphs has been performed through CFD analysis. It has been chosen a representative geometry typical of a regional turboprop aircraft. The typical geometry is very close to ATR-72 geometry and a possible new configuration of a 90 seats regional turboprop (with 5 abreast) called NGTP-5. The geometrical data of the proposed turboprop geometry is summarized in Table 1 and shown in Figure 7. As it is clearly shown in the figure, assuming one fuselage shape, the wing AR, the wing position, the horizontal tailplane size and position and the vertical tail size have been changed to estimate the effect of each component on the interference on side-force vertical tail aerodynamics.

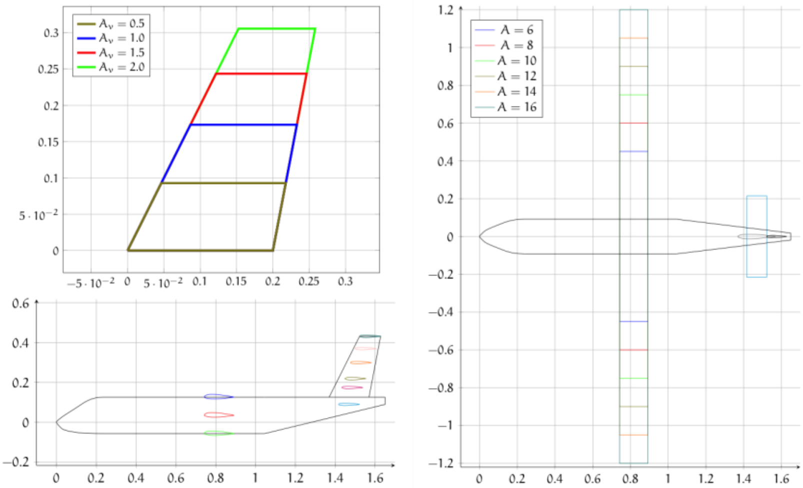

Figure 7: Geometries of the CFD model.

Fuselage parameters				
	fuselage slenderness l_f/d_f	nose ratio l_n/l_f	cone ratio l_c/l_f	wing position $x_{w_{LE}}/l_f$
ATR-72	10.3	1.3	3.2	0.41
NGTP-5	9	1.3	3.3	0.47
CFD model	9	1.3	3.3	0.45

Vertical tail parameters							
	A_v	λ_v	$\Lambda_{v_{LE}}$	$\Lambda_{v_{TE}}$	S_v/S	$x_{v_{LE}}/l_f$	$\bar{V}_v$
ATR-72	1.56	0.61	32°	17°	0.20	0.83	0.098
NGTP-5	1.43	0.63	29°	15°	0.24	0.85	0.110
CFD model	variable	variable	30°	15°	variable	variable	variable

Horizontal tail parameters							
	A_h	λ_h	$\Lambda_{h_{LE}}$	$\Lambda_{h_{TE}}$	S_h/S	$x_{h_{LE}}/l_f$	$\bar{V}_h$
ATR-72	4.1	n. a.	n. a.	n. a.	0.18	n. a.	0.19
NGTP-5	4.1	n. a.	n. a.	n. a.	0.25	n. a.	0.19
CFD model	4.1	0	0°	0°	0.20	variable	variable

Table 1: Characteristics of the model to be investigated by CFD.

Before to attempt any analysis, it was necessary to perform some preliminary tests to define the correct mesh and physics parameters: base size and Reynolds number. The base size is a reference length to which the size of all cells is related. It permits to scale the whole mesh by varying a single parameter. Given the aircraft configuration shown in Figure 8, the most complicated mesh due to the intersections among components, the left part of the figure shows that the optimum base size is 1.65 m, corresponding to about 10 millions of polyhedral cells for that configuration. It has to be noted that twenty prismatic layers have been placed in the boundary layer in order to have an y^+ around one and the residuals value of the RANS equation have been lower than $10e^{-8}$.

Once chosen the base size the study on Reynolds number has been performed. In the lower right part of Figure 8 it is shown the insensitivity to the Reynolds number up to an angle of sideslip of 10°. The turbulence model chosen is Spalart-Allmaras. These results permit to define the sideforce derivative as the ratio of C_Y evaluated at $\beta = 5°$

$$C_{Y\beta v} \approx \frac{C_{Yv}(5°)-0}{5°-0°} = \frac{C_{Yv}(5°)}{5} \text{ deg}^{-1} \quad \text{Eq. 1}$$

4.1 CFD analyses

Having frozen mesh and physics parameter CFD analyses were performed on several configuration, from the isolated vertical tailplane to the complete aircraft. The effect of each component on the vertical tail was evaluated by means of ratios of $C_{Y\beta v}$ between configurations, to highlight the interference. For example, the effect of adding the fuselage to the isolated vertical tail was obtained by dividing the $C_{Y\beta v}$ of the body-vertical configuration by the $C_{Y\beta v}$ of the isolated vertical tail (with the same aspect ratio, planform and mesh parameters).

Due to the high number of mesh cells all analyses were solved on the SCoPE grid infrastructure(see Figure 3). The polyhedral mesh and the Spalart-Allmaras turbulence models were chosen to solve the asymmetrical flow field. All of the runs were solved in incompressible flow, Re = 1000000, at $\alpha = 0°$ and $\beta = 5°$, since the angle of attack is not relevant for directional stability and with a sideslip of 5° the effects are linear, that is the aircraft is in cruise condition. The mesh parameters, common to all analyses, are reported in Table 2. At first the isolated vertical tail has been evaluated to evaluate how and if the Helmold-Diederich[2][4] formula is applicable to this kind of aerodynamic surface.

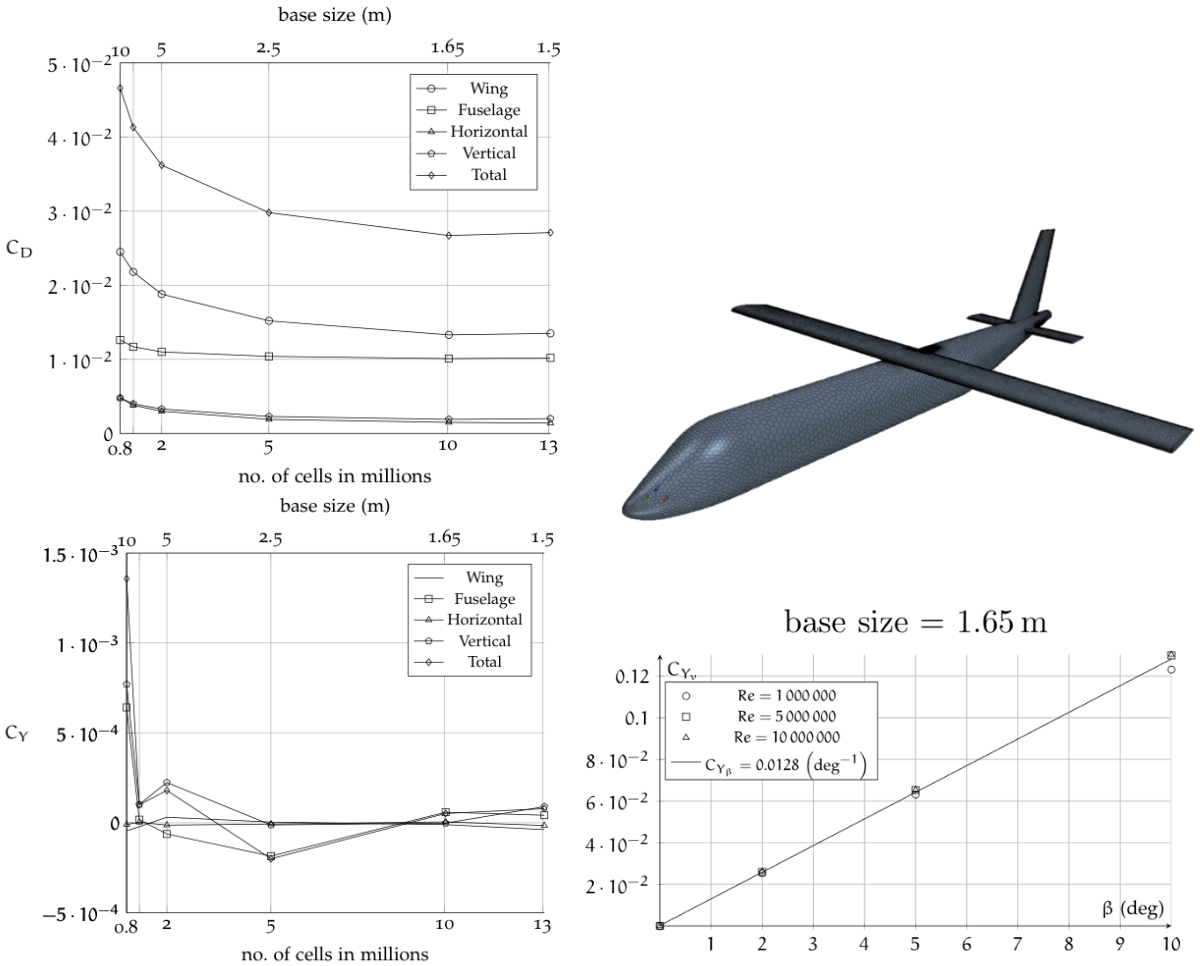

Figure 8: Results of the preliminary tests: variation of the aerodynamic coefficients with base size (left) and insensitivity to Reynolds number (lower right) for the configuration depicted on upper right.

Mesh type	polyhedral cells		
Base size	1.65 m		
Number of prism layers	20		
Prism layer stretching	1.1		
Block shape size	$60 \times 30 \times 20\,\mathrm{m}^3$		
Mesh size (in percentage of the base size)			
	Minimum	Target	Prism layer
Wing	0.04	0.5	0.02
Fuselage	0.1	1.0	0.02
Horizontal	0.04	0.5	0.02
Vertical	0.05	0.5	0.01
Angle of attack α	0°		
Angle of sideslip β	5°		
Reynolds number Re	1 000 000 (based on wing chord)		
Mach number M	0		
Flow regime	fully turbulent (Spalart-Allmaras model)		

Table 2: Mesh and physics data common to all CFD analyses.

4.1.1 Isolated vertical tail

The vertical tail alone has to be analyzed for three reasons: CFD results must verify linearity be compatible with theory and provide the lift gradient $C_{L\alpha v}$. Beyond the vertical tailplane of the CFD model, represented in Figure 7, a rectangular and a constant taper ratio tailplanes were analyzed (as shown in Figure 9). Here it is noted that the CFD model component has a constant sweep angle, but a variable taper ratio, and the behavior predicted by CFD is the same of that predicted by the curves reported in literature(Helmold-Diederich[2][4]), as shown in Figure 10. The rectangular tailplane has only a slightly higher trend respect to the swept one and this is in contrast with theory that provides a much higher lift gradient. The constant taper vertical tailplane does not agree with theory simply because it has variable sweep with aspect ratio and hence it should not be compared at all.

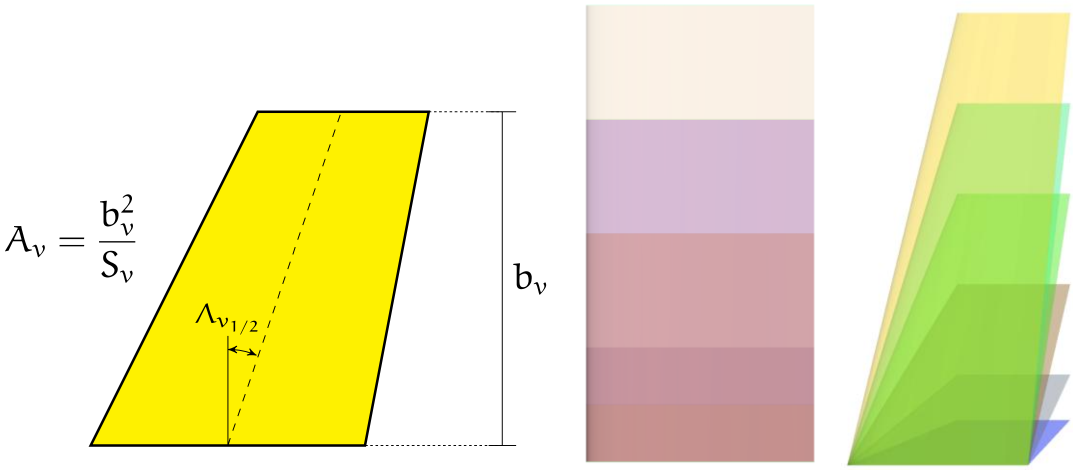

Figure 9: Definition of the parameters of the isolated vertical tail (left). Sequences of straight (center) and constant tapered (right) vertical tailplanes analyzed.

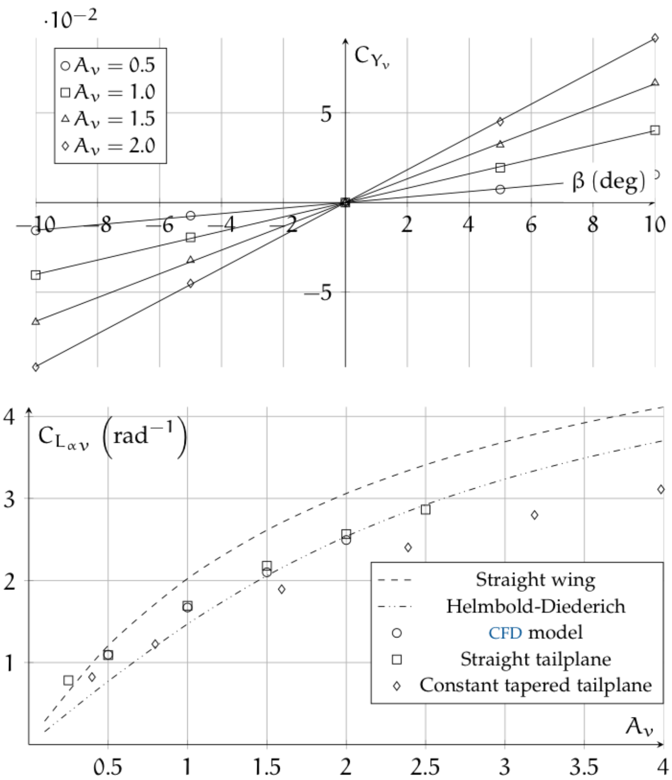

Figure 10: Linearity (up) and compliance with theory (down) for the isolated vertical tails.

4.1.2 Fuselage effect

The first coupling effect studied was that of fuselage. This effect is measured by the ratio between the sideforce coefficients of the body-vertical configurations of Figure 11 left and those of the same isolated vertical tails previously analyzed.

According to Perkins[12] and NACA experiments[8][9] suggest that the fuselage acts as a cylinder at the vertical tail root, accelerating the flow and increasing the sideforce on the vertical tail(Figure 12). Results, in terms of the C_{Y_V} ratios versus $b_v/2r$, are shown in Figure 11 right. Here b_v is the geometric tail span of the isolated vertical tail, not the one defined by Roskam[2], that is there's no tail span extension to the fuselage centerline. The parameter 2r is again the fuselage thickness on the x location of the aerodynamic center of the vertical tailplane. It can be seen a little scatter among different tailplanes of different aspect ratios, sweep angles and taper ratios, even at low $b_v/2r$ ratios (i.e. little tailplanes on a big fuselage), instead of the results of Queijo and Wolhart[9] reported in Figure 13, where there's a bigger data scatter, especially among tails of different aspect ratio.

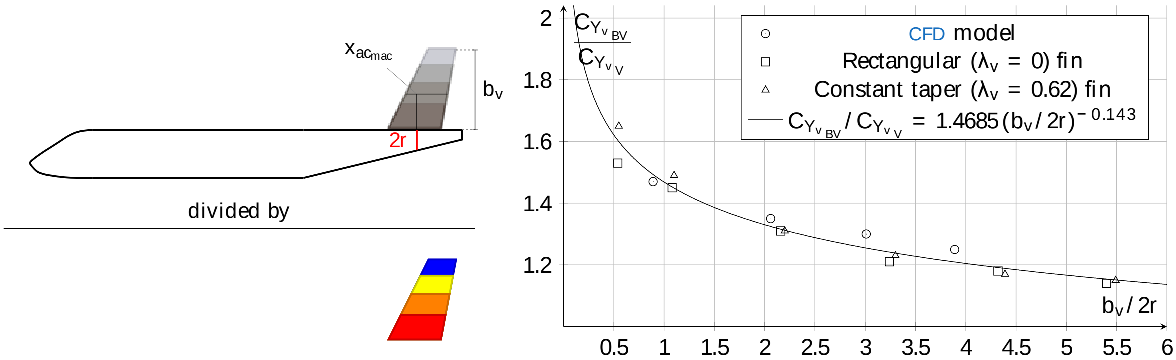

Figure 11: Body effect on vertical tailplane sideforce.

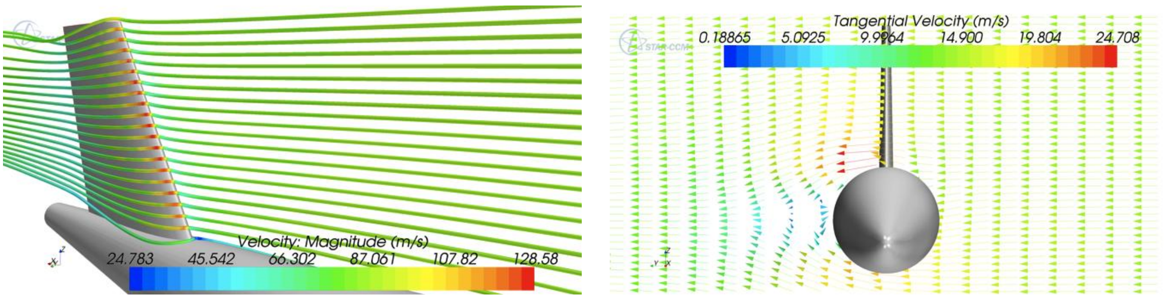

Figure 12: Streamlines (left) and tangential velocity vectors (right) on a transversal section of the vertical tail.

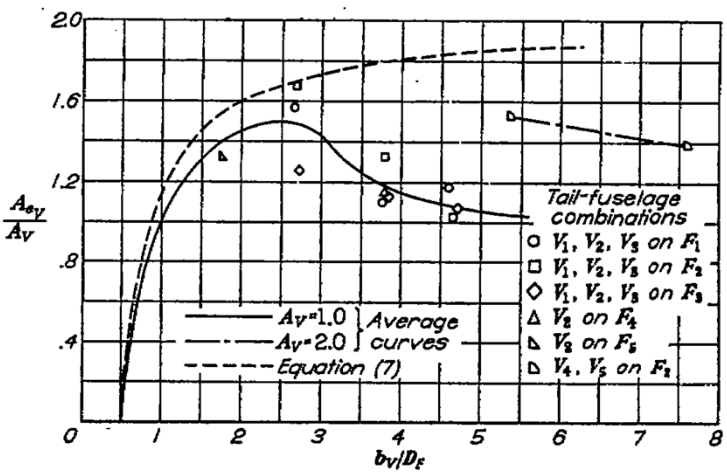

Figure 13: The body effect according to NACA report 1049[9]

4.1.3 Wing effect

The objective of these analyses is the evaluation of the effect of wing position and aspect ratio on the sideforce of the vertical tail. In order to achieve this, several rectangular wings, of different aspect ratio, were simulated at high, mid and low position in fuselage. Combinations involved are depicted in Figure 14, while results are shown – in terms C_{Y_v} ratios between configurations – in Figure 15. The choice of the vertical tailplanes aspect ratios' $A_v = 1$ and $A_v = 2$ is due to consider two extreme values of this parameter: since the scatter between these values is negligible, it can be argued that the effect of the wing on the C_{Y_v} is independent from the choice of the vertical tailplane.

For high wing Figure 15 shows that C_{Y_v} decreases with wing aspect ratio A of about 5%, with respect to the body-vertical configuration.

Mid wing has no effect; it is neutral from a directional point of view, as reported by Perkins and Hage[12]. Data spread (Figure 15) is negligible, around 1% of unity.

For low wing the C_{Y_v} decreases with wing aspect ratio A, probably because of the decreasing magnitude of tip vortices with aspect ratio. In this configuration, however, there's an increase of about 5% of the sideforce coefficient (Figure 15), with respect to the body-vertical configuration.

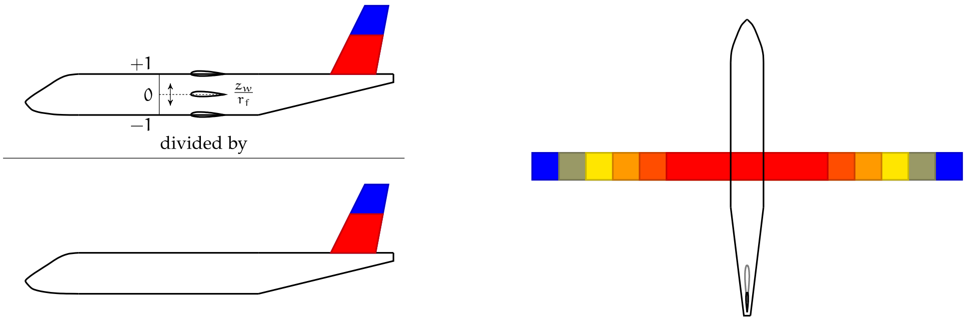

Figure 14: Configurations involved in the analyses of wing effect.

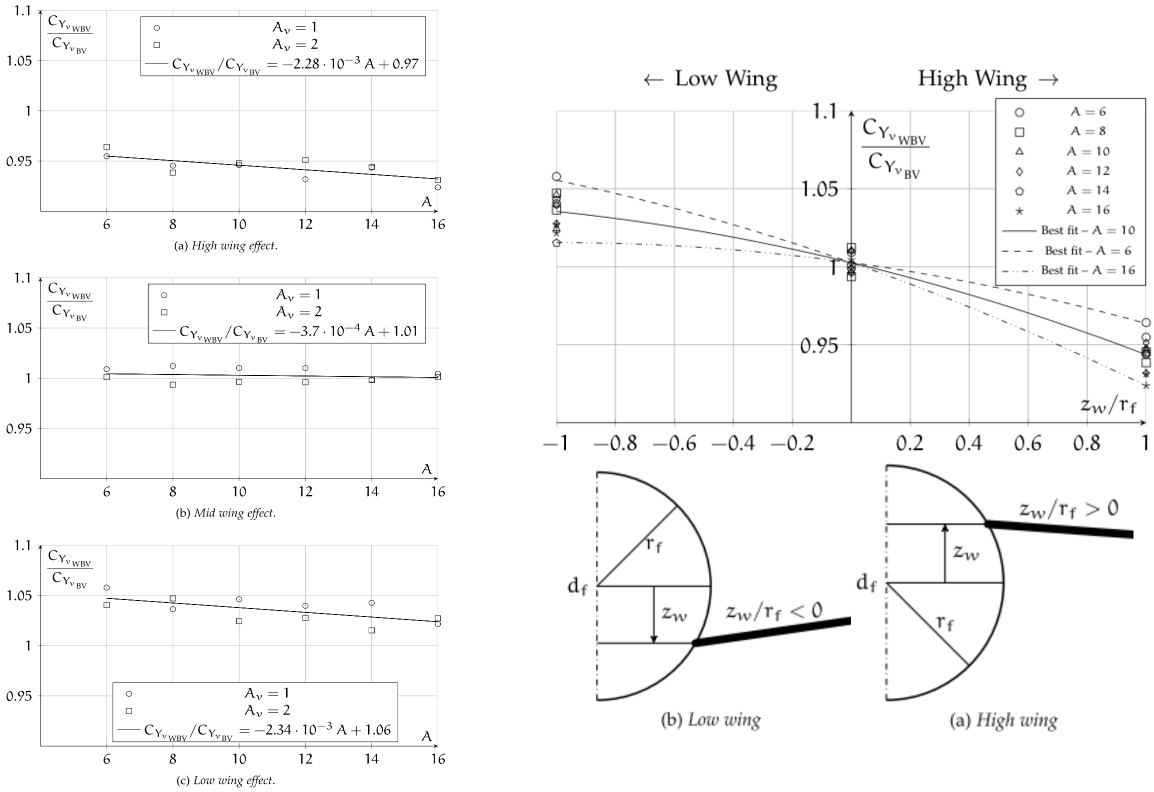

Figure 15: Wing effects; high, mid and low position.

4.1.4 Horizontal tailplane effect

The horizontal tailplane influences the vertical tailplane with its position and size. The former is a major effect, while the latter has a minor influence, especially for tailplanes of the same surface.

A straight horizontal tailplane, of constant size and aspect ratio (Figure 16, Table 1), is mounted in five positions on the fin and one on the fuselage. Then, the same horizontal tailplane, initially centered in chord, is moved forward and rearward by 25% of the local vertical tailplane chord.

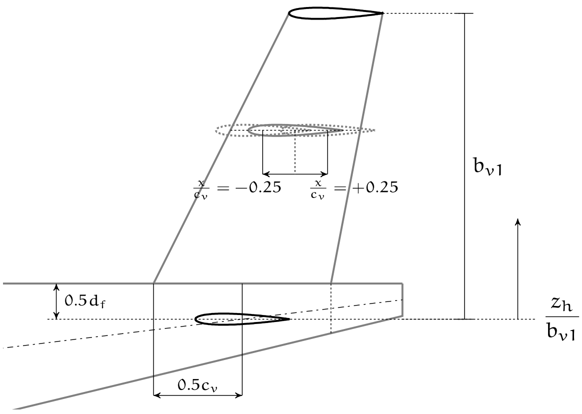

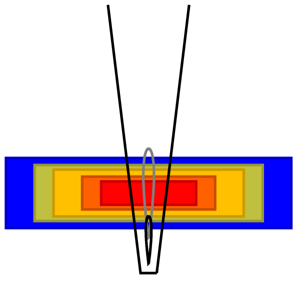

(a) *Variation of* S_h.

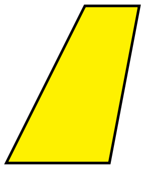

(b) S_v *for* $A_v = 2$.

Figure 16: Configurations involved in the analyses on the horizontal tailplane effect.

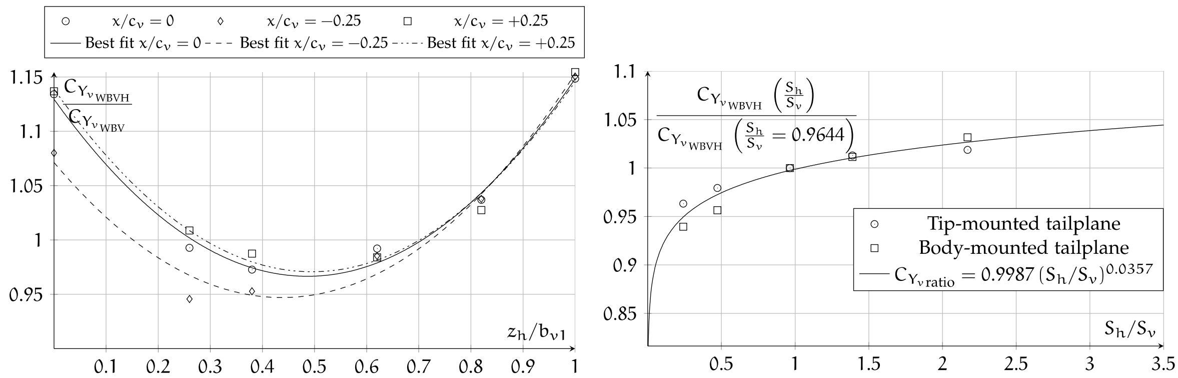

Figure 17: Effect of horizontal tailplane position (left) and size (right)

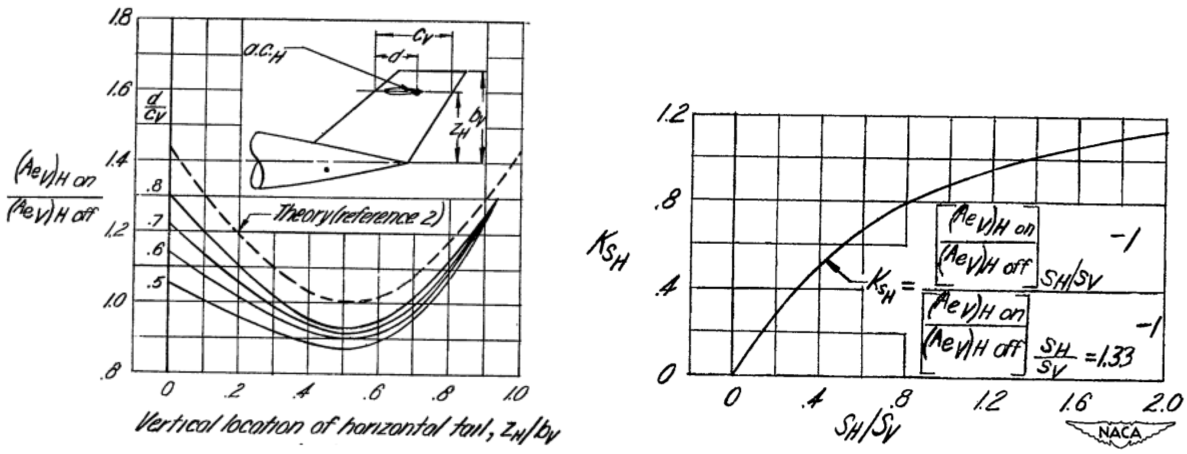

Figure 18: Horizontal tailplane position (left) and size (right) effects, according to Brewer and Lichtenstein[10].

Results are shown in Figure 17 left, in terms of C_{Yv} ratios between the wing-body-fin-horizontal configuration (i.e. the complete airplane) and the wing-body-fin configuration. The trend is much similar to that of Figure 18 by Brewer and Lichtenstein[10], that is the effect of positioning the horizontal tailplane on the fuselage and on the free tip of the vertical tailplane is almost the same. It is apparent that the screening effect of the horizontal tailplane is maximum at extreme positions and decreases moving it forward.

The effect of tailplanes' relative size is shown in Figure 17 right, where it is represented the ratio C_{Yv} between the complete airplane with the horizontal tail varying in size and the previous configuration with a ratio S_h/S_v close to unity (the original horizontal tailplane). Two extreme positions were analyzed, that is the body-mounted and tip-mounted.

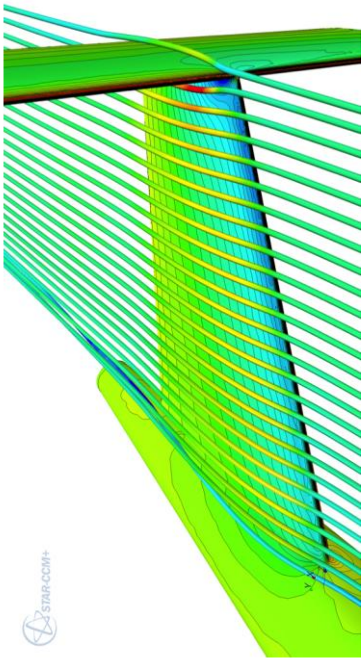

Figure 19: Streamlines and pressure contour on the fin-mounted (T-tail) configuration.

5 Conclusions

The objective of this work was a deep investigation on the vertical tailplane, through the Computational Fluid Dynamics. As a matter of fact, tailplane's design necessarily passes through the determination of the static stability derivatives and the more accurate the latter, the better the former. Two are the main semi-empirical methods used for the determination of the stability derivatives, USAF DATCOM and ESDU. Both of them correct the lift curve slope of the isolated vertical tailplane by means of semi-empirical factors to account for the effect of the fuselage (body), wing and horizontal stabilizer. They are different in how these corrective coefficients act on the lift gradient. Both methods are based on NACA reports of the first half of the '900, though ESDU makes also use of some unpublished data by aircraft industries. So both of them refer to the airplane's shape of the past and tries to link potential flow theory to wind tunnel test, even for high scattered data. These methods have been compared in a stand-alone analysis as well as parametric studies. It appeared that semi-empirical methods give the same results for certain configurations, as the high-winged, T-tail turboprop, but they are less accurate for those configurations (both airliners and commuters) with the horizontal stabilizer mounted in fuselage.

Nowadays computing power permits complex CFD analyses both on desktop computers and cluster grids. For the purpose of this work, the commercial software Star-CCM+ was used, both in local and on the SCoPE University's grid. Several test cases, excerpted from the same NACA reports

to which semi-empirical methods are based, were simulated to verify the compliance of CFD results to the experimental data and the results were comforting. After this compliance, the analyses for the stated investigation were performed. The simulations files were organized to provide the mutual interference among the airplane components. For example, the effects of the fuselage (body) on the vertical tailplane's sideforce coefficient was measured by dividing the sideforce coefficient of the vertical tailplane of the body-vertical configuration by the sideforce coefficient of the isolated tailplane, in the same flow conditions and mesh parameters. Results of these analyses are published as sideforce coefficients ratios among the configurations and best fit curves are provided to mathematically describe the trend exhibited by numerical data. These results show that, according to the trends found in literature, a small tail on a big fuselage exhibits an increase of the sideforce due to sideslip coefficient; another increase is given by a short wing positioned low on fuselage; the horizontal tail has its maximum effect if moved at an extreme position, i.e. body-mounted or tip-mounted (end-plate effect); a smaller effect is the tailplanes' relative sizes, slightly increasing the sideforce of the vertical tail as the horizontal gets bigger.
This results can be very useful in the preliminary design phase, since vertical tail is usually dimensioned by means of statistical and historical data on similarly airplanes. Now trend curves and corrective factors for each aircraft's component are available for prop airliners geometries.

Acknowledgment

The authors wish to thank Prof. A. De Marco for his valid help in setting the SCoPE system for CFD analysis.

References

[1] Finck, R. D. (1978). *USAF Stability and Control DATCOM.* Wright-Patterson Air Force Base, Ohio: McDonnell Douglas Corporation.

[2] Roskam, J. (1997). *Airplane design part VI: preliminary calculation of aerodynamic, thrust and power characteristics.* DAR Corporation.

[3] Gilbey, R. W. (1982). *Contribution of fin to sideforce, yawing moment and rolling moment derivatives due to sideslip, (Yv)F, (Nv)F, (Lv)F, in the presence of body, wing and tailplane.* ESDU.

[4] P. D. Chappell, R. W. Gilbey, et al. *Lift-curve slope and aerodynamic centre position of wings in inviscid subsonic flow*. Item 70011.Engineering Science Data Unit, 1970.

[5] Nicolosi, F., Della Vecchia, P., & Corcione, S. (2012). *Aerodynamic analysis and design of a twin engine commuter aircraft.* ICAS.

[6] Jacobs N. Eastmen and Ward E. Kenneth. *Interferences of wing and fuselage from tests of 209 combinations in the NACA variable density wind tunnel*. Report 540. National Advisory Committee for Aeronautics, 1935.

[7] Rufus O. House and Arthur R. Wallace. *Wind-tunnel investigation of effect of interference on lateral stability characteristics of four NACA 23012 wings, an elliptical and circular fuselage and vertical fins*. Report 705. National Advisory Committee for Aeronautics,1940.

[8] Bamber, R. J., & House, R. O. (1939). *Wind-tunnel investigation of effect of yaw on lateral-stability characteristics. II – Rectangular NACA 23012 wing with a circular fuselage and a fin.* NACA.

[9] Queijo, M. J., & Wolhart, W. D. *Experimental investigation of the effect of the vertical-tail size and length and of fuselage shape and length on the static lateral stability characteristics of a model with 45° sweptback wing and tail surfaces.* 1950: NACA.

[10] Brewer, J. D., & Lichtenstein, J. H. (1950). *Effect of horizontal tail on low-speed static lateral stability characteristics of a model having 45° sweptback wing and tail surfaces.* NACA.

[11] Eastmen, J. N., & Kenneth, W. E. (1935). *Interferences of wing and fuselage from tests of 209 combinations in the NACA variable- density wind tunnel.* NACA.

[12] Perkins, C. D., & Hage, R. E. (1949). *Airplane performance stability and control.* Wiley.

[13] Weber, J., & Hawk, A. C. (1954). *Theoretical load distributions on fin-body-tailplane arrangements in a side-wind.* London, UK: Ministry of Supply.